Distributed Circuit Model for Multi-Color Light-Actuated Opto-Electrowetting Microfluidic Device

Shao Ning Pei, Justin K. Valley, Yi-Lun Wang, and Ming C. Wu, *Fellow, IEEE*

***Abstract*—We report on a distributed circuit model for multi-color light-actuated optoelectrowetting devices. The model takes into consideration the large variation of absorption coefficient (15×) of photoconductors in the visible spectrum and the nonuniform distribution of photogenerated carriers. With the help of this model, we designed opto-electrowetting devices with optimum thickness of photoconductors. This leads to significant improvement in performance compared with prior reports, including 200× lower optical power, 5× lower voltage, and 20× faster droplet moving speed. This enables the use of commercial projectors to create on-demand "virtual" electrodes for large-scale parallel manipulation of droplets. We have achieved simultaneous manipulation of 96-droplet array. Finally, we have demonstrated parallel on chip detection of Herpes Simplex Virus Type 1 within 45 min using a real-time isothermal polymerase chain reaction assay.**

***Index Terms*—Droplet microfluidics, electrowetting, light-actuated digital microfluidics, optoelectrowetting, polymerase chain reaction (PCR).**

I. Introduction

DROPLET-BASED digital microfluidics offers new capabilities for chemical/biological assays. A large number of samples can be processed simultaneously. The small droplet volume greatly reduces the sample and reagent use and increase the sensitivity of detection. There are two primary types of droplet-based microfluidics. The first is surfactant-stabilized water-in-oil emulsions that can be rapidly generated in microfluidic channels [1]–[3], but they can only be addressed/processed sequentially. The other is individually addressable digital microfluidic system such as electrowetting-on-dielectric (EWOD) devices [4]–[7]. Here, each droplet can be independently addressed by voltage, making it possible to perform parallel manipulation of droplets. This paper will focus on the second type of digital microfluidics.

Though several biological and chemical functions have been demonstrated, including glucose assays [8], DNA amplification with polymerase chain reaction (PCR) [9], [10], purification of peptides and proteins from heterogeneous mixtures [11], mammalian cell culturing [12] and chemical synthesis [13], the number of droplets that can be simultaneously processed in EWOD devices is limited by the number of electrodes in two-dimensional arrays. To eliminate the electrical interconnect bottleneck, we have previously proposed opto-electrowetting (OEW) devices that use projected light patterns to turn on "virtual electrode" [14], [15]. The droplet will follow the movement of light. This is made possible by using a photoconductor as light sensitive electrodes. The initial OEW devices still have pixelated electrodes. The subsequent devices used a featureless continuous film of photoconductors, thus decoupling the smallest droplet volume with electrode size [16]. Droplet size as small as 10 pl has been demonstrated. However, these OEW devices require a focused laser beam to move the droplets, unlike the optoelectronic tweezers that can be powered by commercially available digital light projectors [17], [18]. Substantial reduction of the optical power density requirement (from 250 W/cm^2) is needed since the light intensity available from typical projects is around 1.4 W/cm^2. Though droplet manipulation using digital projector has been reported, the droplets were trapped in the dark gap between two illuminated areas in lateral devices with very high operating voltages [19].

A new challenge arises when using projector to power OEW devices. Since projectors are designed for display, they produce light with multiple colors over the entire visible regime. The optical absorption coefficient in typical photoconductors such as amorphous silicon varies by as much as an order of magnitude from red to blue spectra. Blue light is absorbed within 0.3 μm while red light penetrates several micrometers. The distribution of photo-generated carriers is therefore highly non-uniform. The previous model that treats the photoconductor as a lumped variable resistor completely breaks down. Color based studies of optoelectronics tweezers device has been reported by Lin *et al.* [20] and Liang *et al.* [21], but their study is limited to optically induced dielectrophoresis with very different requirements. Hence, a detailed optimization study of the a-Si:H layer's switching ability with respect to the projector's color spectrum and power output will be able to provide very useful insights into optimum device design in layer thicknesses and maximum droplet actuation force.

In this paper, we report on a distributed circuit model that takes into consideration color dependence and the non-uniform distribution of photo-generated carriers. Using this model, we have derived the optimum thickness of photoconductors for

Manuscript received December 23, 2014; revised January 26, 2015; accepted February 8, 2015. Date of publication March 2, 2015; date of current version July 13, 2015. This work was supported in part by the Berkeley Sensor and Actuator Center and DARPA iMDs Program award # HR0011-12-2-0003.

The authors are with the Berkeley Sensor and Actuator Center, Department of Electrical Engineering and Computer Sciences, University of California, Berkeley, CA 94720 USA (e-mail: shaoning@eecs.berkeley.edu; valleyj@gmail.com; yilun@berkeley.edu; wu@eecs.berkeley.edu).

This paper has supplementary downloadable material available at http://ieeexplore.ieee.org. The supplementary material contains two video files. S1.m1v shows the sequential dispense of 18 droplets from the reservoir. S2.m1v shows the 96 droplet array formation. The total size of the files are 10.2 MB.

Color versions of one or more of the figures in this paper are available online at http://ieeexplore.ieee.org.

Digital Object Identifier 10.1109/JLT.2015.2405076

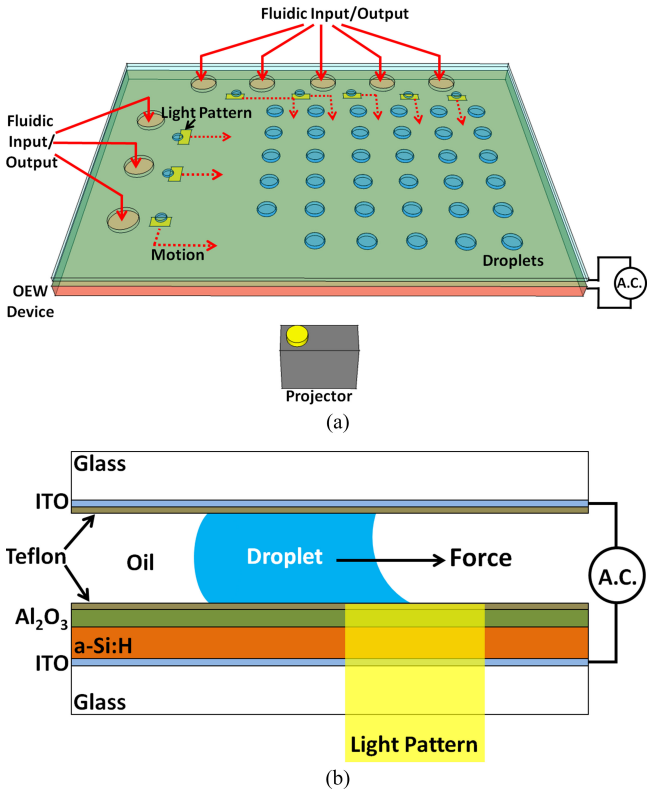

Fig. 1. (a) Schematic of the light-actuated digital microfluidic device. The droplets are transported by projected light patterns from a digital light projector. (b) Device schematic showing incident light creating a localized area of high conductivity in the a-Si:H film. This switches the voltage drop from the a-Si:H layer to the oxide layer. A net electro-mechanical force then acts on the droplet, translating it toward the light pattern.

given output spectra of selected projectors. This has resulted in 200x reduction in the optical power requirement and enabled us to design an optimized OEW device powered by digital projectors. We have demonstrated droplet moving speed >1 cm/s, parallel manipulation of 96 droplets, and detection of Herpes Simplex Virus (HSV) using an isothermal PCR assay.

II. Device Design and Methods

A. Design and Operation

Fig. 1 illustrates the structure and operating principle of the device. The device (bottom) consists of an indium-tin-oxide (ITO)-coated glass substrate, a photoconductive layer of hydrogenated amorphous silicon (a-Si:H), a dielectric layer of aluminum oxide (Al_2O_3), and a thin hydrophobic layer of Teflon AF. The top layer consists of an ITO- and Teflon-coated glass substrate. The microfluidic droplet manipulation chamber is defined between the top and bottom substrates with a spacer. An ac voltage is applied between the top and bottom ITO layers. In the absence of light, the applied ac voltage drops primarily across the highly resistive a-Si:H layer. Upon illumination, the conductivity of the a-Si:H increases by more than 10× [22]. This shifts the voltage drop to primarily across the dielectric layer. In other words, the a-Si:H layer acts as a photo-activated switch that turns on/off the voltage across the dielectric layer. Thus, the illuminated area is analogous to an electrically biased electrode, or a "virtual electrode". If the virtual electrode is created only on part of the droplet's contact line, a net electromechanical force [23], [24] acts on the droplet and translates it towards the illuminated region, achieving the OEW effect.

B. Methods

We use 300-nm ITO-coated glass substrates, a 0.1–1.5 μm thick photoconductive a-Si:H layer deposited via plasma-enhanced chemical vapor deposition (Oxford Plasmalab 80plus), a 100-nm Al_2O_3 deposited by atomic layer deposition (ALD) (Picosun Sunale R150) and a 25 nm spin-coated (3000 r/min, 30 s) 0.2% Teflon AF film (Dupont, Wilmington, DE, USA) for the OEW device. The top electrode is made of another Teflon-coated ITO glass wafer. The fabrication process does not require any photolithography. The two substrates are bonded face-to-face with a spacer layer of double-sided tape (50–1000 μm), forming a microfluidic chamber.

During operation, an ac voltage is applied between the two ITO electrodes. A commercially available digital projector (Dell 4210X DLP) is used as spatial light modulator for generating light patterns. The projected area is 1.6 cm × 1 cm, and the resulting pixel is 10 μm × 10 μm on the device. The liquid droplets could be actuated with one or multiple pixels at a time. Optical patterns are generated on a computer. Bright-field illumination, a continuous zoom microscope (Navitar 12X), and a CCD camera (Sony XCD-X710) are used for visualization and recording. No external optical lenses other than those from the projector and microscope are required. During operation, the fluidic chamber is first filled with silicone oil (1.0 cSt DMS Trimethylsiloxy-terminated Polydimethylsiloxane, Gelest Inc. Morrisville, PA). Aqueous droplets (10 mS/m deionized water with added KCl) are then introduced into the fluidic chamber via a syringe pump (KD Scientific, 780210) and Teflon tube (Cole-Parmer Microbore PTFE). The oil surrounding the aqueous droplets reduces the friction during movement as well as minimizes the evaporation of the droplets.

The actuation voltage is inversely proportional to the areal capacitance of the dielectric layer [25]–[28]. Therefore, the actuation voltage can be reduced by using thinner insulator and/or insulator with higher dielectric constant. Advances in ALD have made it possible to deposit high quality, conformal, pinhole-free layers of dielectric films on the devices. Hence, ALD is a good candidate for scaling down dielectric thickness to increase actuation force. However, there is a fundamental limit on the minimum thickness because of dielectric breakdown [25]. Here, we use 100 nm thick aluminum oxide (Al_2O_3) for our dielectric film. It has a high dielectric constant (∼10) and a high breakdown field (∼500 MV/m).

III. Optimization

For efficient OEW actuation, the thickness of the photoconductor should be optimized. In previous analysis [16], [17], the photoconductor was modeled as a lumped variable resistor whose resistance changes with incident light intensity. In the physical device, however, the photogenerated carriers are not distributed uniformly in the photoconductor. They follow the

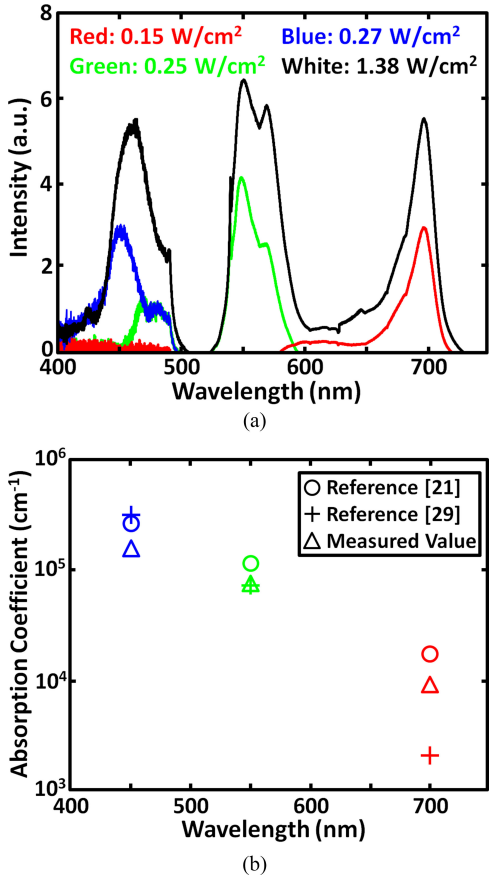

Fig. 2. (a) The output spectra and power densities of the projector used in this experiment (Dell 4210X). White light output is 2× stronger than the combined red, green and blue light due to the design of the projector's color wheel. (b) Absorption coefficients of amorphous silicon measured at blue, green and red color. Data from literature is also plotted for comparison.

distribution of the light intensity, which decays exponentially from the surface. The decay length is the inverse of the absorption coefficient, which is usually a sensitive function of the wavelength. The output of a digital projector covers the entire visible spectrum. Therefore, a much more detailed model is needed to correctly predict the performance of OEW.

We have characterized the output spectra and power density of the projector used in our experiment (Dell 4210X DLP). Fig. 2(a) shows the spectra when the projector is programmed to produce red, green, blue and white colors (Princeton Instruments SP2750). The power densities, measured by a thermopile at a distance of 7 cm from the projector, are 0.15, 0.25 and 0.27 W/cm^2 for red, green, and blue light, respectively. The power density of white light (1.38 W/cm^2) is about twice of the combined powers of red, green and blue light due to the design of the color wheel and operation of the DLP chip. The measured and reported [21], [29] absorption coefficient for hydrogenated amorphous silicon (a-Si:H) is shown in Fig. 2(b). The wavelength band is simplified to be 450 nm for blue, 550 nm for green, and 700 nm for red. It varies by an order of magnitude across the visible spectrum: the absorption coefficient for blue wavelength, α_{blue}, is measured to be 15× higher than that for red wavelength, α_{red}.

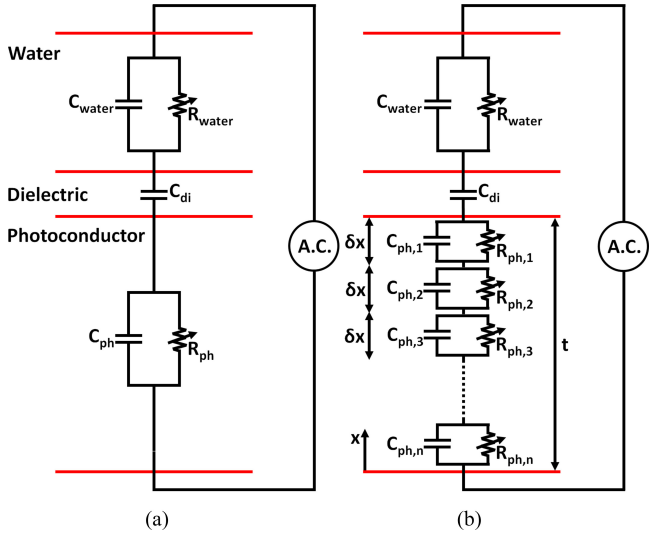

Fig. 3. (a) Lumped element equivalent circuit used to model previous OEW devices. (b) The distributed circuit model proposed here to account for the color dependence and non-uniform distributions of photo-generated carriers.

Previously, the photoconductor was modeled as a parallel combination of a variable resistor, R_{ph}, and a capacitor, C_{ph} (see Fig. 3(a)). Our distributed model is shown in Fig. 3(b). The photoconductor consists of many infinitesimal slices of thickness δx, each slice is modeled as a parallel combination of a resistor $R_{\mathrm{ph}}(x) = \rho(x)\,\delta x$ and a capacitor $C_{\mathrm{ph}}(x) = \varepsilon_0\varepsilon_{\mathrm{ph}}/\delta x$, where x is the distance from the surface of the photoconductor facing the projector, $\rho(x)$ is the resistivity of the photoconductor, ε_0 is the free-space permittivity, and $\varepsilon_{\mathrm{ph}}$ is the relative dielectric constant of the photoconductor. The ac impedance of the slice per unit area is therefore:

$$Z_{\delta x}(x) = \frac{\rho(x)\,\delta x}{1 + j\omega\varepsilon_{\mathrm{ph}}\varepsilon_0\rho(x)} \tag{1}$$

where ω is the ac frequency. The light intensity decays exponentially inside the photoconductor due to absorption:

$$I(x) = I_0 e^{-\alpha x} \tag{2}$$

where α is the absorption coefficient of the photoconductor. The local distribution of the projected red, green, blue light at a certain depth x are plotted in Fig. 4(a) using the measured power density and the measured blue (450 nm), green (550 nm), and red (700 nm) absorption coefficients shown in Fig. 2(b). The blue and green light are attenuated much faster than red light in aSi:H. The intensity distribution of white light and "dark" output is also shown in the same plot. It should be mentioned that the projector still output a small amount of light even in the dark state (when the color of the projector is set to black).

The local electron and hole concentrations, $\delta n(x)$ and $\delta p(x)$, are related to the carrier generation rate $G_{\delta x}$:

$$G_{\delta x}(x) = \frac{I_0}{h\upsilon\delta x}\left(e^{-\alpha x} - e^{-\alpha(x+\delta x)}\right) \tag{3}$$

$$\delta n(x) = G_{\delta x}(x)\,\tau_n \tag{4}$$

$$\delta p(x) = G_{\delta x}(x)\,\tau_p \tag{5}$$

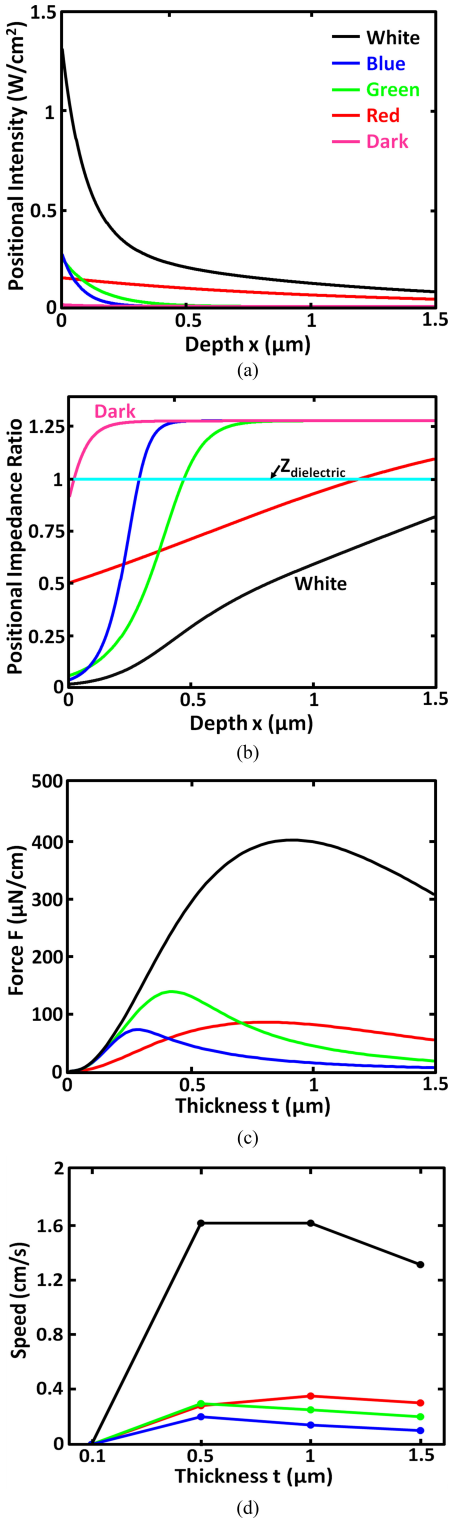

Fig. 4. (a) Optical intensity distribution in amorphous silicon photoconductor for various color light from the projector. Blue and green is attenuated rapidly while red light penetrates more than 1.5 μm. (b) Local impedance versus distance from the illuminated surface for amorphous silicon under various color light from the projector. The impedance is normalized to that of the dielectric layer. (c) The calculated force per unit length imparted on the droplet versus the thickness of a-Si:H for various color light from the projector (white, red, green, blue). The optimum thickness for white light is about 0.91 μm. (d) The measured maximum velocity of the droplet versus the thickness of the amorphous silicon under various color light from the projector. The general trends agree well with the theoretical prediction.

where h, υ, τ_{n}, τ_{p} are the Planck's constant, optical frequency, electron and hole lifetimes, respectively. For simplicity we assume 100% internal quantum efficiency and 100% optical transmittance at all interfaces.

The resistivity at location x is:

$$\rho(x) = \frac{1}{q\mu_n \delta n(x) + q\mu_p \delta p(x)} \tag{6}$$

where μ_n and μ_p are the electron and hole mobility, respectively. The local impedance at a certain depth x, normalized to the impedance of the dielectric layer, is shown in Fig. 4(b) for various color illuminations. Here, low impedance means the illuminated spot is turned on. Fig. 4(b) clearly shows that blue and green lights are much more effective in turning on the photoconductor (i.e., reducing the total impedance), but only for thin photoconductors ($d < 0.28$ μm for blue light, and <0.45 μm for green light).

The total impedance, $Z_{\mathrm{ph,total}}$, for a photoconductor with thickness t can be calculated by integrating $Z_{\delta x}(x)$:

$$Z_{\mathrm{ph,total}} = \int_0^t Z_{\delta x}(x)\mathrm{dx}. \tag{7}$$

The applied voltage is split between the ALD dielectric layer and the photoconductor. The impedance of the dielectric layer is:

$$Z_{\mathrm{di}} = \frac{1}{j\omega C_{\mathrm{di}}} \tag{8}$$

where C_{di} is the capacitance of the ALD layer per unit area. The voltage drop across the dielectric layer can be calculated using a voltage divider:

$$V_{\mathrm{di}} = \frac{Z_{\mathrm{di}}}{Z_{\mathrm{di}} + Z_{\mathrm{ph,total}}}. \tag{9}$$

Finally, as only the advancing half of a droplet is illuminated during droplet actuation. Force imparted on a droplet is calculated to be the advancing side's force (light) minus off the unilluminated trailing side's force (dark). The actuation force per unit length of the contact line, F, can be calculated as [24]:

$$F = \frac{1}{2}\frac{\varepsilon_{\mathrm{di}}\varepsilon_o}{t_{\mathrm{di}}}\left(V_{\mathrm{di,light}}^2 - V_{\mathrm{di,dark}}^2\right) \tag{10}$$

where $\varepsilon_{\mathrm{di}}$, t_{di} are the relative permittivity and thickness of the dielectric layer, respectively. $V_{\mathrm{di,light}}$ and $V_{\mathrm{di,dark}}$ are the voltage dropped across the dielectric layer, calculated from equation (9), when the photoconductor is illuminated with and without light, respectively.

The droplet actuation force per unit length for a given thickness of a-Si:H is calculated for projected light with different colors for an OEW device with 100 nm Al_2O_3 and an ac frequency of 10 kHz, using incident light intensity I_0 in Fig. 2(a). The calculated force as a function of photoconductor thickness t is plotted in Fig. 4(c). From the plot, it can be seen that a-Si:H thickness of 0.28, 0.41, and 0.8 μm imparts the most force on the droplet for blue, green and red light, respectively. White light's force is significantly stronger due to its higher incident power.

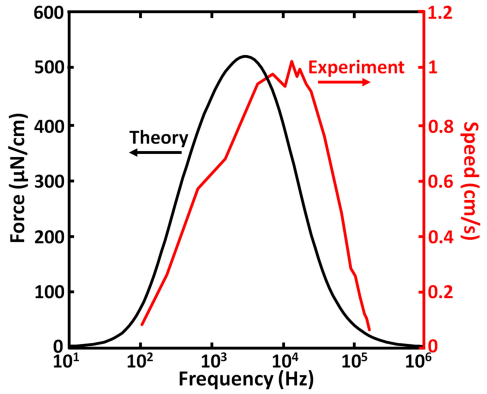

Fig. 5. The calculated force and the measured maximum speed of 190 nl droplets versus the frequency of the ac bias for an OEW device with 300 μm height and biased at 40 V_{ppk}.

IV. Experimental Demonstrations and Application

A. Optimization Model Verification

To validate the new model, OEW devices with different a-Si:H thicknesses (0.1, 0.5, 1 and 1.5 μm) are fabricated. The Al_2O_3 thickness is kept at 100 nm. The maximum droplet actuation speeds are measured with a bias of 40 V_{ppk} voltage at 10 kHz frequency. The microfluidic chamber height is 300 μm and the conductivity of the liquid is 10 mS/m. The measured results shown in Fig. 4(d) are in good agreement with the theoretical model in Fig. 4(c). The ratio of the measured speeds under white light and single-color light actuation is higher than that predicted by the theoretical model. The difference might be due to the friction experienced by the droplet [30].

The distributed model enables us to optimize the OEW device design and reduce optical power requirement by 200×. The power reduction allows us to use standard data projector rather than a focused laser beam. Droplet speed of more than 1 cm/s is observed consistently in samples with 0.5 to 1 μm thick a-Si:H under white light illumination. Although the analysis is carried out with a specific light source and device parameters, changes can be easily incorporated for different light sources/devices.

B. Droplet Motion Dependence on AC Frequency

An ac voltage bias is needed to transport droplet in the device, because in the dc state, all voltage will drop across the dielectric layer (open circuit) even if photoconductivity is varied. To determine the best ac frequency, we used the same model to calculate the frequency response of the device, as shown in Fig. 5. The best response is observed at around 10 kHz. This agrees well with experimentally measured maximum speed of 190 nL droplets at an applied voltage of 40 V_{ppk}, which is also shown in Fig. 5.

C. Droplet Dispensing From Reservoir

The ability to create droplets from on-chip reservoirs is important for lab-on-a-chip applications. The reservoirs here are defined optically. Their areas are usually much larger than individual droplets. Fig. 6 shows three snapshots of a video clip demonstrating the droplet generation process. 120 nl droplets are generated at a rate of 0.18 droplet/sec using a moving light pattern with an area of 1 mm × 1 mm (see video S1).

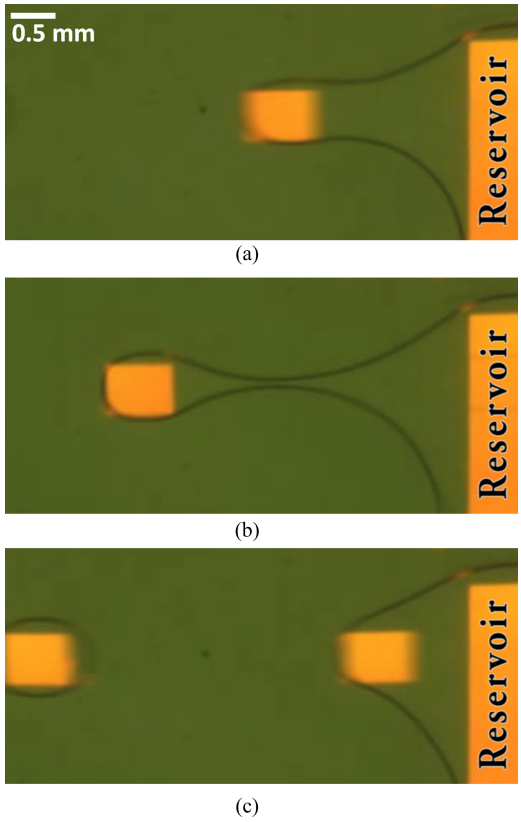

Fig. 6. Snap shots of a video clip showing dispensing 120 nl droplets from an optically defined reservoir. One droplet is generated every 5.5 s. The OEW device is biased with 60 V_{ppk} at 10 kHz.

D. Droplet Array Formation

High-density array of droplets enable high throughput multiplexed assays. Fig. 7 demonstrates the device's ability to form 96-droplet (8 × 12) array. Light patterns extract 220-nl droplets dispensed from a Teflon tube and arrange the droplets in rows of 12 before transporting them into a rectangular array (see video S2).

These demonstrations show the OEW device is well suited to directly miniaturize and automate biological or chemical analysis currently performed using well plates and pipettes. This will greatly reduce the amount of reagent used as well as the reaction time. The process can be automated to reduce the amount of manual labor and incubation time.

E. Biomedical Application in Viral Detection

Herpes Simplex is a common sexually transmitted disease caused by Herpes Simplex Virus (HSV). In recently years, Helicase-dependent isothermal PCR detection of HSV has been demonstrated (BioHelix Corporation, Beverly, MA, USA) [31]. Real-time PCR is performed by heating the assay to 64 °C and the presence of HSV can be detected using fluorescence read

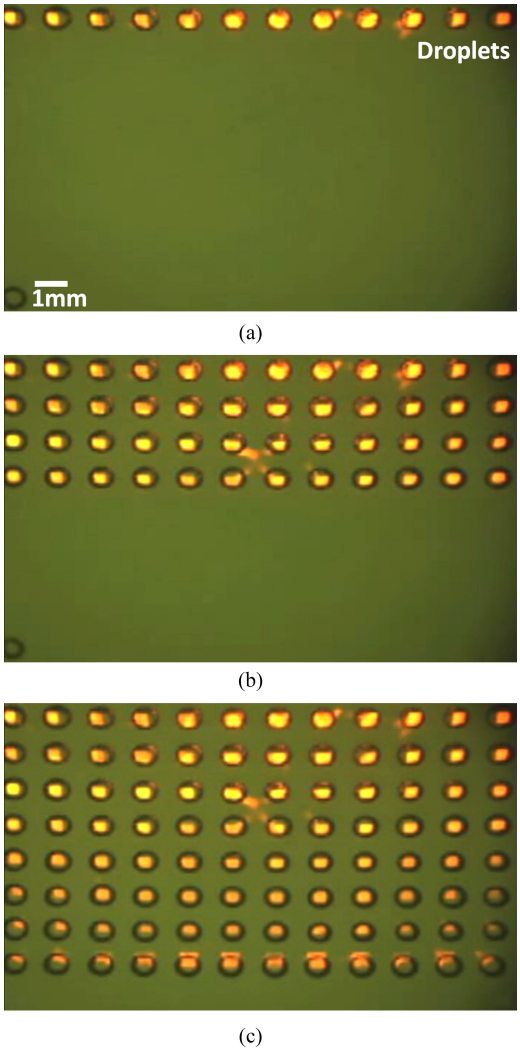

Fig. 7. Snapshots of a video clip showing the formation of 96 (8×12) droplet array by OEW acutuation. The 220 nl droplets are dispanced by a syringe pump and a Teflon tube. The OEW device is baised with 60 V_{ppk} at 10 kHz.

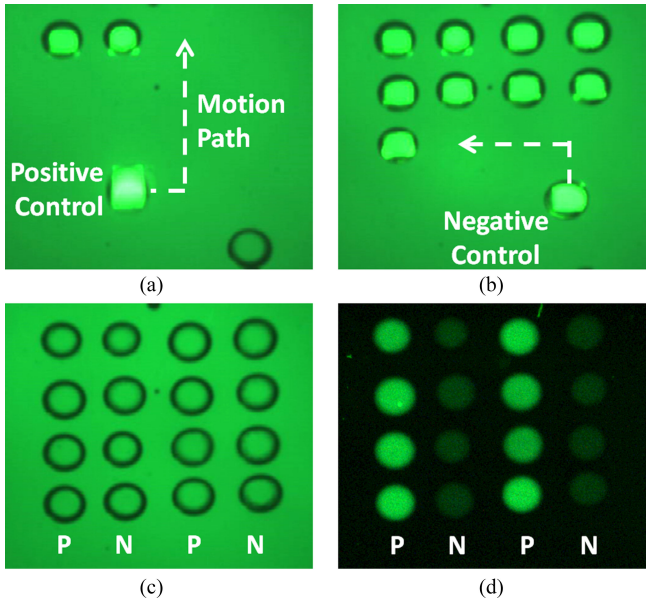

Fig. 8. (a)–(c) Positive and negative control droplets were dispensed from tubes and transported into array position. The negative control droplets contain blank viral transport medium while the positive control droplet contain 1.45×10^3 viral-particles/nl. The first and the third columns are positive control droplets while the second and the fourth columns are negative control. (d) The fluorescence image of the final amplified products after 45 min at 64 °C. No cross contamination was observed.

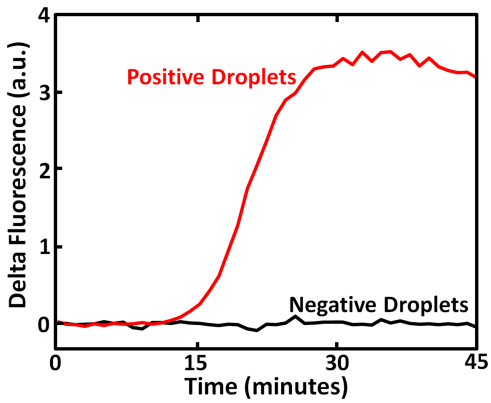

Fig. 9. The average fluorescence reading versus time for the eight positive and eight negative control droplets. The fluorescence is normalized to the baseline fluorescence reading.

out. The OEW device is a good candidate for conducting this detection assay—with parallel readouts of indexed samples.

HSV Type 1 (MacIntyre Strain) purified viral lysate was acquired from Advanced Biotechnologies (Columbia, MD), Helicase-dependent PCR kit (IsoAmpIII tHDA) and blank viral transport medium were acquired from Biohelix (Beverly, MA, USA), forward and reverse primers were acquired from Integrated DNA Technologies (Coralville, IA, USA), and were designed to target and amplify a 100 base pairs (bp) region of the HSV's glycoprotein B gene [32]. EvaGreen fluorescence dye was acquired from Biotium Corp. (Hayward, CA, USA) and ROX reference dye was acquired from Life Technologies (Carlsbad, CA, USA). Isothermal PCR master mix is prepared using assay preparation protocol from "One-Step qHDA" provided by BioHelix, except without component of DNA Template. Pluronic F-68 T 0.2% concentration (Sigma Aldrich, St. Louis, MO, USA) surfactant is added to master mix to prevent non-specific protein adsorption onto the device surface [33].

A 4×4 array was formed using pre-mixed droplets of 400 nl each. The array includes eight positive samples with PCR master mix and 1.45×10^3 viral-particles/nl HSV viral lysate, and eight negative control droplets with PCR master mix and blank viral transport medium. Positive and negative control droplets were dispensed from tubes sequentially and subsequently arranged in a 4×4 array format by OEW (see Fig. 8(a)–(c)).

Fig. 8(d) shows that positive control droplets (columns 1 and 3, denoted by "P") displayed fluorescence, indicating HSV DNA amplification and detection. No negative control droplets showed DNA amplification (columns 2 and 4, denoted by "N") displayed amplification. In Fig. 9, the average fluorescence reading of the eight positive and eight negative control droplets are recorded over time. It shows that only positive control droplets

exhibit fluorescence signals. Droplets were extracted from the chip after the PCR reaction and gel electrophoresis confirmed that the amplified DNA product was 100 bp (data not shown).

V. Conclusion

We have presented a distributed model for light response of photoconductor in OEW device. This model correctly predicts the optimum thickness of photoconductor when used with a multi-color light source, such as a digital light projector. The optimized OEW device has 200× lower optical power requirement than previous devices. The ability to use digital light projector greatly reduces the cost and complexity of the light-actuated digital microfluidic systems. Droplet speed > 1 cm/s is consistently achieved. Droplet inputs from optically defined reservoirs have been realized. We have also demonstrated real-time detection of HSV using isothermal PCR. This light-actuated digital microfluidics platform offers many advantages over other droplet manipulation methods, including versatility and flexibility of the programmable microfluidic systems and the simplicity and low cost of the consumables.

Acknowledgment

The authors would like to thank the Berkeley Marvell Nanolab, where all devices were fabricated, K. Li for help with spectrometry study of projector output, and S. Lim for help with gel electrophoresis.

References

[1] D. N. Adamson, D. Mustafi, J. X. Zhang, "Production of arrays of chemically distinct nanolitre plugs via repeated splitting in microfluidic devices," *Lab Chip*, vol. 6, pp. 1178–1186, 2006.

[2] J. Clausell-Tormos, D. Lieber, J.-C. Baret, A. El-Harrak, O. J. Miller, L. Frenz, J. Blouwolff, K. J. Humphry, S. Köster, H. Duan, C. Holtze, D. A. Weitz, A. D. Griffiths, and C. A. Merten, "Droplet-based microfluidic platforms for the encapsulation and screening of mammalian cells and multicellular organisms," *Chem. Biol.*, vol. 15, no. 5, pp. 427–437, 2008.

[3] L. Mazutis, J. Gilbert, W. L. Ung, D. A. Weitz, A. D. Griffiths, and J. A Heyman, "Single-cell analysis and sorting using droplet-based microfluidics," *Nature Protocols*, vol. 8, pp. 870–891, 2013.

[4] M. G. Pollack, R. B. Fair, and A. D. Shenderov, "Electrowetting-based actuation of liquid droplets for microfluidic applications," *Appl. Phys. Lett.*, vol. 77, pp. 1725–1726, 2000.

[5] S. K. Cho, H. Moon, and C.-J. Kim, "Creating, transporting, cutting, and merging liquid droplets by electrowetting-based actuation for digital microfluidic circuits," *J. Microelectromech. Syst.*, vol. 12, pp. 70–80, 2003.

[6] S. Teh, R. Lin, L. Hung, and A. P. Lee, "Droplet microfluidics," *Lab Chip*, vol. 8, pp. 198–220, 2008.

[7] M. Abdelgawad and A. R. Wheeler, "The digital revolution: A new paradigm for microfluidics," *Adv. Mater.*, vol. 21, pp. 920–925, 2009.

[8] V. Srinivasan, V. K. Pamula, and R. B. Fair, "Droplet-based microfluidic lab-on-a-chip for glucose detection," *Analytica Chimica Acta*, vol. 507, pp. 145–150, 2004.

[9] Z. Hua, J. L. Rouse, A. E. Eckhardt, V. Srinivasan, V. K. Pamula, W. A. Schell, J. L. Benton, T. G. Mitchell, and M. G. Pollack, "Multiplexed real-time polymerase chain reaction on a digital microfluidic platform," *Anal. Chem.*, vol. 82, no. 6, pp. 2310–2316, 2010.

[10] Y. Chang, G.-B. Lee, F. Huang, Y. Chen, and J. Lin, "Integrated polymerase chain reaction chips utilizing digital microfluidics," *Biomed. Microdevices*, vol. 8, pp. 215–225, 2006.

[11] A. R. Wheeler, H. Moon, C. A. Bird, R. R. Loo, C. J. Kim, J. A. Loo, and R. L. Garrell, "Digital microfluidics with in-line sample purification for proteomics analyses with MALDI-MS," *Anal. Chem.*, vol. 77, pp. 534–540, 2005.

[12] I. Barbulovic-Nad, S. H. Au, and A. R. Wheeler, "A microfluidic platform for complete mammalian cell culture," *Lab Chip*, vol. 10, pp. 1536–1542, 2010.

[13] J. R. Millman, K. H. Bhatt, B. G. Prevo, and O. D. Velev, "Anisotropic particle synthesis in dielectrophoretically controlled microdroplet reactors," *Nature Mater.*, vol. 4, pp. 98–102, 2005.

[14] P. Y. Chiou, H. Moon, H. Toshiyoshi, C. J. Kim, and M. C. Wu, "Light actuation of liquid by optoelectrowetting," *Sens. Actuators A, Phys.*, vol. 104, no. 3, pp. 222–228, 2003.

[15] P. Y. Chiou, Z. Chang, and M. C. Wu, "Droplet manipulation with light on optoelectrowetting device," *J. Microelectromech. Syst.*, vol. 17, pp. 133–138, 2008.

[16] P. Y. Chiou, S.-Y. Park, and M. C. Wu, "Continuous optoelectrowetting for picoliter droplet manipulation," *Appl. Phys. Lett.*, vol. 93, pp. 221110–221113, 2008.

[17] P. Y. Chiou, A. T. Ohta, and M. C. Wu, "Massively parallel manipulation of single cells and microparticles using optical images," *Nature*, vol. 436, pp. 370–372, 2005.

[18] A. T. Ohta, P.-Y. Chiou, T. H. Han, J. C. Liao, U. Bhardwaj, E. R. B. McCabe, F. Yu, R. Sun, and M. C. Wu, "Dynamic cell and microparticle control via optoelectronic tweezers," *J. Microelectromech. Syst.*, vol. 16, no. 3, pp. 491–499, 2007.

[19] S.-Y. Park, M. A. Teitell, and P.-Y. Chiou, "Single-sided continuous optoelectrowetting (SCOEW) for droplet manipulation with light patterns," *Lab. Chip.*, vol. 10, pp. 1655–1661, 2010.

[20] W.-Y. Lin, Y.-H. Lin, and G.-B. Lee, "Separation of micro-particles utilizing spatial diffference of optically induced dielectrophoretic forces," *Microfluidics Nanofluidics*, vol. 8, pp. 217–229, 2000.

[21] W. Liang, S. Wang, Z. Dong, G.-B. Lee, and W. J. Li, "Optical spectrum and electric field waveform dependent optically-induced dielectrophoretic micro-manipulation," *Micromach.*, vol. 3, pp. 492–508, 2012.

[22] J. K. Valley, A. Jamshidi, A. T. Ohta, H.- Y. Hsu, and M. C. Wu, "Operational regimes and physics present in optoelectronic tweezers," *J. Microelectromech. Syst.*, vol. 17, pp. 342–350, 2008.

[23] F. Mugele and J. Baret, "Electrowetting: From basics to applications," *J. Phys., Condens. Matter*, vol. 17, pp. 705–774, 2005.

[24] T. B. Jones, J. D. Fowler, Y. S. Chang, and C. J. Kim, "Frequency-based relationship of electrowetting and dielectrophoretic liquid microactuation," *Langmuir*, vol. 19, pp. 7646–7651, 2003.

[25] H. Moon, S. K. Cho, R. L. Garrell, and C. J. Kim, "Low voltage electrowetting-on-dielectric," *J. Appl. Phys.*, vol. 92, pp. 4080–4087, 2002.

[26] Y. Li, W. Parkes, L. I. Haworth, A. A. Stokes, K. R. Muir, P. Li, A. J. Collin, N. G. Hutcheon, R. Henderson, B. Rae, and A. J. Walton, "Anodic Ta_2O_5 for CMOS compatible low voltage electrowetting-on-dielectric device fabrication," *Solid-State Electron.*, vol. 52, no. 9, pp. 1382–1387, 2008.

[27] J.-H. Chang, D. Choi, S. Han, and J. Pak, "Driving characteristics of the electrowetting-on-dielectric device using atomic-layer-deposited aluminum oxide as the dielectric," *Microfluidics Nanofluidics*, vol. 8, pp. 269–273, 2010.

[28] Y.-Y. Lin, R. D. Evans, E. Welch, B.-N. Hsu, A. C. Madison, and R. B. Fair, "Low voltage electrowetting-on-dielectric platform using multi-layer insulators," *Sens. Actuators B*, vol. 150, no. 1, pp. 465–470, 2010.

[29] Y. Hishikawa, S. Tsuge, N. Nakamura, S. Tsuda, S. Nakano, and Y. Yukinori, "Device-quality wide-gap hydrogenated amorphous silicon films deposited by plasma chemical vapor deposition at low substrate temperatures," *Jpn. J. Appl. Phys.*, vol. 69, pp. 508–510, 1991.

[30] V. Bahadur and S. V. Garimella, "An energy-based model for electrowetting-induced droplet actuation," *J. Micromech. Microeng.*, vol. 16, no. 8, p. 1494, 2006.

[31] M. D. Poulter, H. Kong, Y.-W. Tang, and B. Yen-Lieberman, "A rapid and simple isothermal nucleic acid amplification test for detection of herpes simplex virus types 1 and 2," *J. Clin. Virol.*, vol. 50, pp. 26–30, 2011.

[32] Y. Tong, K. McCarthy, H. Kong, and B. Lemieux, "Development and comparison of a rapid isothermal nucleic acid amplification test for typing of herpes simplex virus types 1 and 2 on a portable fluorescence detector," *J. Mol. Diagn.*, vol. 14, no. 6, pp. 569–576, 2012.

[33] V. N. Luk, G. C. H. Mo, and A. R. Wheeler. "Pluronic additives: A solution to sticky problems in digital microfluidics," *Langmuir*, vol. 24, no. 12, pp. 6382–6389, 2008.

Shao Ning Pei received the B.S. degree in electrical engineering from the University of Michigan, Ann Arbor, MI, USA, in 2009, and the M.S. degree in electrical engineering from the University of California, Berkeley, CA, USA, in 2011, where he is currently working toward the Ph.D. degree in electrical engineering at the Electrical Engineering and Computer Science Department, Berkeley Sensor and Actuator Center. His research interests include the areas of microfluidics, optofluidics, single-cell analysis, and microelectromechanical systems.

Justin K. Valley received the B.S. degree in electrical engineering from the University of Michigan, Ann Arbor, MI, USA, in 2006, and the M.S. and Ph.D. degrees in electrical engineering from the University of California, Berkeley, CA, USA, in 2008 and 2011, respectively. From 2011 to 2014, he was with the DLP Products division of Texas Instruments, Dallas, TX, USA, where he was involved in the development of next generation nonoptical MEMS technology. In 2014, he joined Berkeley Lights, Inc., Emeryville, CA, where he is involved in the definition and productization of a variety of technological platforms for the biotechnology sector.

Yi-Lun Wang received the B.S. degree in physics and the M.S. degree in electrical and electronics engineering from National Taiwan University, Taipei City, Taiwan, in 2009 and 2013, respectively.

Ming C. Wu (F'02) received the B.S. degree in electrical engineering from National Taiwan University, Taipei City, Taiwan, and the M.S. and Ph.D. degrees in electrical engineering and computer sciences from the University of California, Berkeley, CA, USA, in 1986 and 1988, respectively.

From 1988 to 1992, he was a Member of Technical Staff at AT&T Bell Laboratories, Murray Hill, NJ, USA. From 1992 to 2004, he was a Professor of electrical engineering at the University of California, Los Angeles. He has been a Faculty Member at Berkeley since 2004. He is a Nortel Distinguished Professor of electrical engineering and computer sciences at the University of California, Berkeley. He is also the Codirector of the Berkeley Sensor and Actuator Center and the Faculty Director of UC Berkeley Marvell Nanolab. His research interests include semiconductor optoelectronics, nanophotonics, MEMS, and optofluidics. He has published eight book chapters, more than 500 papers in journals and conferences, holds 22 U.S. patents.

Dr. Wu was a Packard Foundation Fellow from 1992 to 1997. He received the 2007 Paul F. Forman Engineering Excellence Award from the Optical Society of America.